Vibration Measurement and Wave Reflection Analysis in an Electrified Railway Catenary Based on Analytical Methods

Fuchuan Duan, *Student member, IEEE,* Zhigang Liu, *Senior Member, IEEE,*

Yang Song, *Member, IEEE,* Stefano Derosa, Anders Rønnquist and Donghai Zhai

Abstract— The wave propagation property of the catenary directly affects the pantograph–catenary interaction performance. Specifically, wave reflection and transmission occurring at waveguide discontinuities, particularly at dropper junctions, directly impact the pantograph–catenary interaction performance. In this study, wave reflection occurring at the dropper junctions are investigated using both analytical and experimental approaches. First, a partial catenary model is established to analyze the catenary wave propagation by considering the wave reflections at the dropper junctions. Result indicates that the wave reflection in the contact wire (CW) affects the contact performance more significantly than that in the messenger wire. Two types of experimental tests are performed to analyze the wave reflection in the catenary—single CW and full-scale catenary tests. An analytical method considering back-and-forth reflections between the adjacent droppers is proposed to identify the actual reflection coefficients and extract the wave components from the measured data. The single CW test result shows that the dropper mass has a negligible influence on the wave reflection. The full-scale catenary test result indicates that the catenary reflection coefficient obtained from the measured data can match the design value with an acceptable error using the proposed method. Moreover, the measured data can be decomposed into wave components with different reflection orders, in which less energy is centered in the higher-reflection-order component. The proposed methods have been justified effective in reflection coefficient identification for the actual catenary structure.

*Index Terms—*Electrified railway, Catenary, Vibration measurement, Wave reflection, Wave decomposition, Reflection coefficient

I. Introduction

TENSIONED cable systems are widely used in many engineering structures, most of which are subjected to uniform loads such as gravity and wind loads. The electrified catenary is a special application of the tensioned cable system subjected to moving loads induced by pantographs. Owing to the high flexibility of railway catenaries, wave propagation

F. Duan and Z. Liu are with the School of Electrical Engineering, Southwest Jiaotong University, Chengdu 610031, China (E-mail: duanfc_cd@outlook.com, liuzg_cd@126.com).

D. Zhai is with the Department of Software Engineering, Southwest Jiaotong University, Chengdu 610031, China (E-mail: dhzhai@swjtu.edu.cn)

Y. Song, S. Derosa, and A. Rønnquist are with the Department of Structural Engineering, Norwegian University of Science and Technology, 7491 Trondheim, Norway (E-mail: y.song_ac@hotmail.com, stefano.derosa@ntnu.no, and anders.ronnquist@ntnu.no).
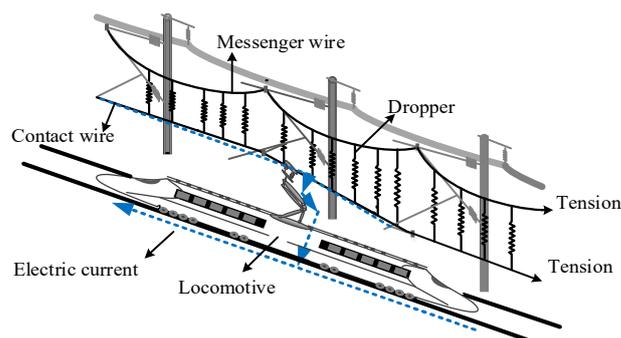
Fig. 1 Electric railway pantograph and catenary system

plays an important role that affects the contact quality between the catenary with pantographs.

Typically, a catenary is a two-level tensioned cable structure established along the railroad and mainly comprises the contact wire (CW) and messenger wire (MW) connected by several droppers (Fig. 1). The catenary is often the only source of power for electric locomotives. The current collection quality primarily depends on the sliding contact performance between the moving pantograph and catenary, which can be evaluated by the contact force fluctuation between the registration strip of the pantograph and CW of the catenary. The contact force fluctuation must be retained as low as possible to ensure a stable electric transmission from the catenary to the locomotive engine. Nowadays, the dynamic behavior of the tensioned cable system subjected to a moving load has attracted considerable research attention, as it has the potential to solve practical problems in various engineering phenomena, such as the pantograph–catenary and vehicle–bridge interactions.

The contact quality between the tensioned cable and moving load is generally affected by the vibration at the contact point caused by the moving load and mechanical wave traveling along the cable [1]. Several studies have provided theoretical foundations for investigating the dynamic contact problem between the tensioned cable structures and moving loads [2-6]. For high-speed railways, the mechanical wave in the catenary is initiated by the moving pantographs and travels along the CW, with reflections and transmissions at discontinuities. Recently, many researchers have investigated pantograph–catenary dynamic responses based on numerical simulations. Among them, the finite element method is the most preferred method to model the catenary [7-12] because it can effectively describe the initial configuration and geometrical nonlinearity. Some

environmental perturbations have been involved in the numerical model, such as the wind load [13,14], track irregularities [15,16], and wire corruption [17-19]. Apart from numerical approaches, experimental tests have been performed to identify the structural damping [20], detect catenary part defect [21], and analyze CW irregularity [22,23]. To improve the current collection, Xu et al. [24] optimized the interval of double pantographs. Some studies have focused on improving the catenary dynamic response measurement methods, which include the contact-type and noncontact methods. The contact-type sensors have been widely used to determine the catenary acceleration under different impacts [20, 25-27]. Further, the noncontact methods based on photogrammetric devices have been established to measure the catenary uplift without interrupting the railway operation [28,29]. In our previous publications, both the contact-type [30] and noncontact methods [31] have been developed for catenary dynamic behavior measurements. And the work in this paper can be regarded as a follow-up research on our previous work in [30] and [31].

Most current research works have focused on upgrading the modeling accuracy and numerical or experimental analysis results. The deterioration of the current collection quality has seldom been studied. The contact force directly originates from the relative vertical displacement between the panhead and CW at the contact point. For the catenary, the vibration of the contact point has two sources—the forced vibration initiated by the moving pantograph and propagating wave. The propagating wave contributes to the fluctuation of the contact point and directly affects the contact quality. An attractive topic in wave propagation in the catenary is investigating the wave reflection and transmission at the dropper point. For instance, Song et al. [32] adopted an analytical model to study the wave reflection at the dropper point and revealed the existence of dominant wave frequencies attributed to the Doppler effect, which can induce system resonance. Other studies have indicated that the contact force variation between the pantograph and CW is mainly caused by both the stiffness variation along the span and wave reflection at the dropper joints, where wave reflection majorly induces the contact loss [33,34].

Generally, for a dropper with negligible damping negligible and infinite stiffness, the wave reflection coefficient at the dropper junction in CW is defined as follows [35].

$$r_d^{cw} = \frac{2\sqrt{S_{mw}\rho_{mw}} + i\omega M_d}{2\sqrt{S_{mw}\rho_{mw}} + 2\sqrt{S_{cw}\rho_{cw}} + i\omega M_d} \quad (1)$$

where the subscripts mw and cw denote MW and CW, respectively, S and ρ are the tension and linear density, respectively, M_d is the mass of the dropper clamp, and ω is the angular frequency, and i is the imaginary unit. Equation (1) provides an essential reference for estimating the reflectivity of a single dropper with respect to the traveling wave. However, for catenaries in service, the classical equation cannot quantify the wave components, including the incident, reflection, and transmission waves, caused by multiple reflections and bidirectional transmissions within several adjacent droppers.

Most existing studies on the catenary wave reflection have mainly focused on demonstrating the reflection phenomenon based on simulation methods [32][36]. In the work of Van et al. [37], a series of mass drop tests was performed on the catenary, based on which the wave reflection induced by droppers was effectively investigated in combination with an analytical model. Based on a combination of field tests and simulation model, Cho [25] proposed a formula to address nonlinear droppers and investigated the effects of wave reflection coefficients on the forces acting on the dropper. However, only limited studies have considered multiple reflections induced by droppers and the actual reflection coefficient identification from the field measurements.

Based on these discussions, in this study, the wave reflection occurring in the catenary is analyzed using field measurements and analytical methods. The main contributions of this study are listed:

(1) A novel analytical method is proposed for extracting the wave components from the composite acceleration history obtained in a single CW test, which can be used to evaluate the wave reflection induced by the discontinuity in the catenary mass.

(2) The reassembled catenary models are established using adjacent droppers considering the reflective cavity with a finite reflection order. Based on the reassembled models and proposed analytical methods, the actual reflection coefficients of the catenary are identified and the wave components at the observation site with different reflection orders are extracted.

The remainder of this study is organized as follows. In Section II, the influence of the reflection coefficients on the catenary uplift is analyzed using the partial model. The CW reflection coefficient has a more pronounced effect on the catenary vibration intensity. In Section III, a series of tests is designed to investigate the influence of the dropper mass on the wave reflection. The single CW is considered separately to avoid the mutual effect arising from MW. In Section IV, field measurements are performed on the full-scale catenary structure and wave reflections occurring at the droppers are analyzed considering the interaction between CW and MW.

II. ANALYSIS OF WAVE TRANSMISSION BETWEEN MW AND CW

Wave reflection and diffraction are known to occur at waveguide discontinuities, such as mass joints and stiffness mutation sites. Different from that in the isolated cable, the wave propagation in the catenary is considerably more complicated. For the catenary, CW is in direct contact with the moving pantograph, through which the electric current is transmitted to the locomotive. Thus, the CW vibration initiated by pantograph excitation propagates along the catenary, reflecting at the dropper joints and traveling to MW via the dropper connection (Fig. 2).
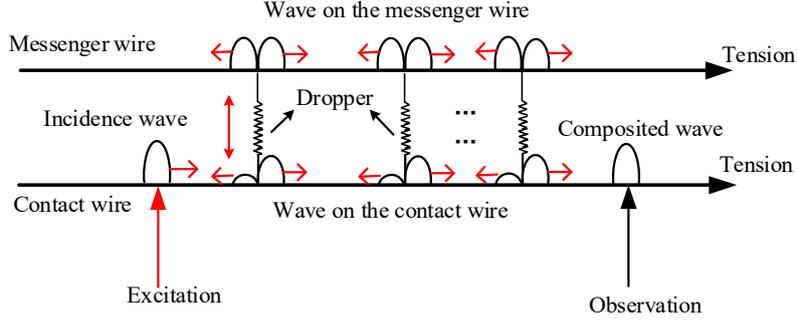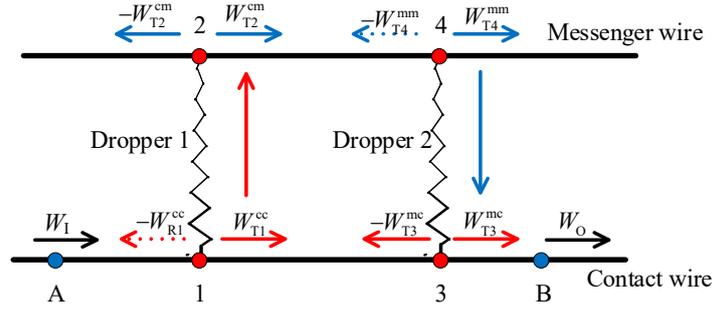
Fig. 2 Waves traveling in the catenary structure.

Fig. 3 Waves propagating back and forth in a local catenary section.

TABLE I
DEFINITIONS OF SUPERSCRIPTS IN FIG. 3

Superscript	Definition	Superscript	Definition
cc	Waves propagating in CW	mm	Waves propagating in MW
cm	Waves propagating from CW to MW through the dropper	mw	Waves propagating from MW to CW through the dropper

Fig. 3 depicts the waves transmitting back and forth between the two wires, where numbers 1, 2, 3, and 4 refer to the dropper junctions in the wires. The subscripts I, R, and T denote the incident, reflection, and transmission waves, respectively. The superscripts cc, cm, mm, and mw denote the waves propagating in different directions (Table I).

The incident wave can be expressed as $W_I = A_I e^{i\omega t}$. For a catenary with an infinite stiffness dropper, the wire motions at Junctions 1 and 2 are synchronized. Then, the compositional waves at Junctions 1 and 2 can be expressed as follows:

$$\begin{bmatrix} W_{T1}^{cc} & -W_{R1}^{cc} \\ W_{T2}^{cm} & -W_{T2}^{cm} \end{bmatrix} = \begin{bmatrix} 1-r_d^{cw} & -r_d^{cw} \\ 1-r_d^{cw} & -1+r_d^{cw} \end{bmatrix} \cdot A_I e^{i\omega t}, \quad (2)$$

where r_d^{cw} is the reflection coefficient at the dropper junction in CW, A_I is the amplitude of the incident wave, ω is the angular frequency, and t is the wave traveling time.

Similarly, the compositional waves at Junctions 4 and 3, which are generated by W_{T2}^{cm}, can be expressed as follows:

$$\begin{bmatrix} W_{T4}^{mm} & -W_{R4}^{mm} \\ W_{T3}^{mc} & -W_{T3}^{mc} \end{bmatrix} = \begin{bmatrix} 1-r_d^{mw} & -r_d^{mw} \\ 1-r_d^{mw} & -1+r_d^{mw} \end{bmatrix} \cdot W_{T2}^{cm}, \quad (3)$$

where r_d^{mw} is the reflection coefficient at the dropper junction in MW. Note that the waves traveling in CW and MW have different speeds owing to different tensions and linear densities. Thus, Equations (2) and (3) can be modified as follows:

$$\begin{bmatrix} W_{T1}^{cc} & W_{R1}^{cc} \\ W_{T2}^{cm} & -W_{T2}^{cm} \end{bmatrix} = \begin{bmatrix} 1-r_d^{cw} & -r_d^{cw} \\ 1-r_d^{cw} & -1+r_d^{cw} \end{bmatrix} \cdot W_I \cdot e^{-i\omega l/v_{cw}} \quad (4)$$

$$\begin{bmatrix} W_{T4}^{mm} & -W_{R4}^{mm} \\ W_{T3}^{mc} & -W_{T3}^{mc} \end{bmatrix} = \begin{bmatrix} 1-r_d^{mw} & -r_d^{mw} \\ 1-r_d^{mw} & -1+r_d^{mw} \end{bmatrix} \cdot W_{T2}^{cm} \cdot e^{-i\omega l/v_{mw}}, \quad (5)$$

where l is the dropper interval and v_{mw} and v_{cw} are the wave speeds in MW and CW, respectively.

Point B is examined to observe the composite signal W_O. Because of multiple wave reflections and diffractions between two droppers, W_O is a time-varying wave in different stages of wave propagation. In the first stage, W_O is the summation of the two waves transmitting from A → 1 → 3 → B and A→ 1 → 2 → 4 → 3 → B. In this stage, the reflection wave between the adjacent junctions has no effect on W_O. Thus, W_O can be expressed as follows:

$$\begin{aligned} W_O &= W_{T3}^{cc} + W_{T3}^{mc} \\ &= \left(1-r_d^{cw}\right) \cdot W_{T1}^{cc} \cdot e^{-i\omega l/v_{cw}} + \left(1-r_d^{mw}\right) \cdot W_{T2}^{cm} \cdot e^{-i\omega l/v_{mw}} \\ &= \left(1-r_d^{cw}\right)\left[\left(1-r_d^{cw}\right)e^{-i\omega l/v_{cw}} + \left(1-r_d^{mw}\right)e^{-i\omega l/v_{mw}}\right] \cdot W_I \end{aligned} \quad (6)$$
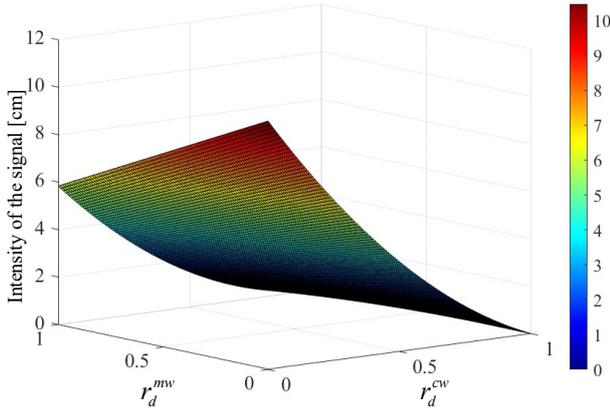
Fig. 4 The intensity of W_O versus r_d^{cw} and r_d^{mw}.

Fig. 4 presents the intensity of W_O versus the reflection coefficients r_d^{cw} and r_d^{mw}. The wave intensity at Point B changes more significantly with r_d^{cw}, while the wave reflection in MW has a lower influence on it. Thus, in Sections III and IV, the wave reflection is primarily investigated using the single CW and full-scale catenary experimental tests.

III. WAVE REFLECTION IN ISOLATED CW

The mass discontinuity of the catenary caused by the dropper clamps is an important factor contributing to the wave reflection. In this study, investigations are performed on the wave reflection occurring in the catenary starting with the single CW vibration tests. In these tests, contact-type sensors are used to measure the dynamic response of CW under impulse force and simulate the mass discontinuity by transferring the extra mass to CW.

A. Experimental setup of single CW test

The experimental setup of the single CW vibration test performed in the laboratory is presented in Fig. 5, in which a standard CW is used as the test object, with the ends of CW fixed [30]. Two fabricated wireless sensors are attached to the wire [20] and work as response collectors and lumped masses. In this test, an impulse is provided using a hammer and the acceleration is measured using the sensors. The main parameters of the tested CW are listed in Table II. The CWs with two tensions are evaluated in the experiment to analyze the effect of tension on the reflection coefficient. The weight of each sensor is 0.39 kg, which nearly corresponds to the weight of a real-life dropper and can be used to quantify the effect of lumped mass on the wave reflection in a real-life catenary.
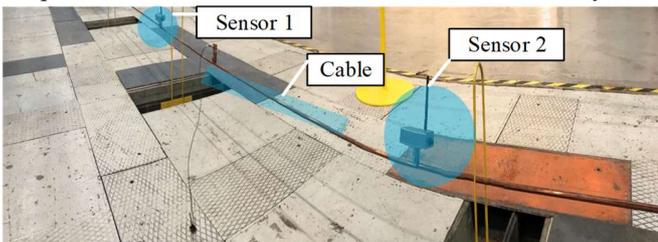

Fig. 5 Experimental setup of a single CW test with two attached sensors.

TABLE II
PARAMETERS OF THE SINGLE CW TEST

Symbol	Quantity	Value
S	Tension	13/15 kN
m	Weight of a single sensor	0.39 kg
x_1	Distance of Sensor 1 from the left side	4.795 m
x_2	Distance of Sensor 2 from the left side	7.300 m
L	Cable length	10.136 m
ϕ	Contact wire section	120 mm²

B. Wave decomposition based on the analytical method

The reflection coefficient of the traveling wave at the joints can be expressed as follows:

$$r = \frac{A_R}{A_I}, \qquad (7)$$

where r is the reflection coefficient and A_R and A_I are the amplitudes of the reflection and incident waves, respectively. However, only the composite wave is obtained in the experimental test shown in Fig. 5, which is a mixed signal of the incident and reflection waves. Fig. 6 presents a schematic of the complex wave propagation in the single CW test. The ideally fixed ends of CW allow it to work as an enclosed reflective cavity, in which multiple wave components exist because of the back-and-forth reflection of the initiated wave at both ends. Moreover, the wave components, which have the same frequency but different phases, reflect and diffract when passing the sensors.

Fig. 7 shows the time history and spectrum of the acceleration obtained using Sensor 1 with 15-kN tension. The signal acquired using Sensor 1 is a superposition of different wave components. Thus, the most challenging aspect of reflection coefficient identification is separating the incident and reflection waves from the composite signal.
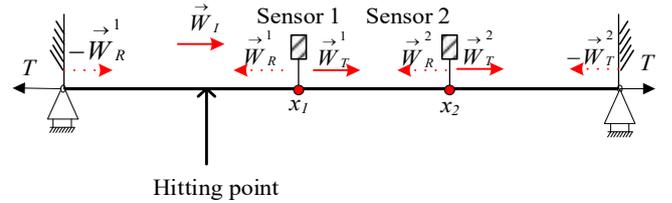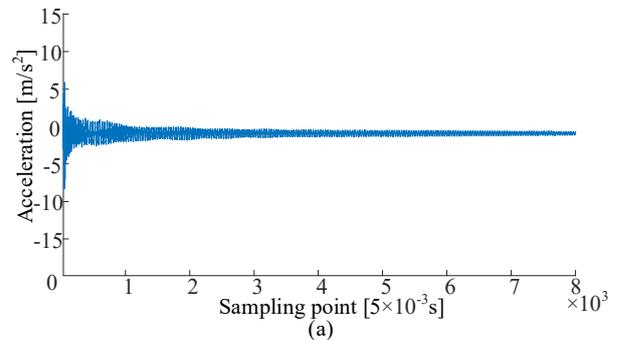

Fig. 6 Waves traveling in the cable. Subscripts R and T denote wave reflection and transmission, respectively. Superscripts 1 and 2 denote the waves influenced by Sensors 1 and 2, respectively.
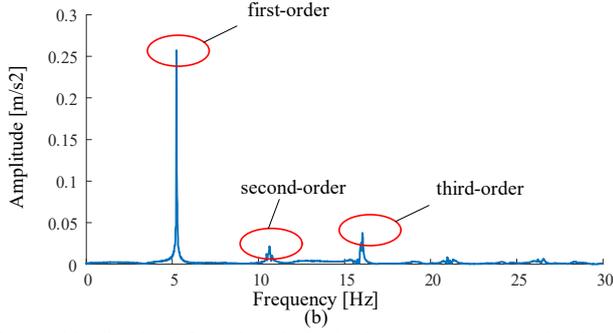

(a)

Fig. 7 Cable vibration information obtained using Sensor 1. (a) Acceleration. (b) Frequency.
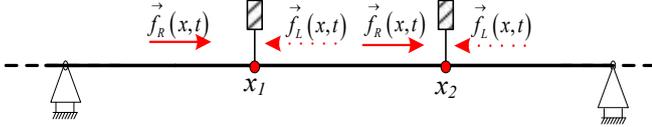

Fig. 8 Waves traveling in the cable using a simplified model.

For the single CW test, the wave components have two propagation directions—left and right. To simplify the calculation, the complex wave propagation in Fig. 6 is reduced to a simple model in Fig. 8. The waves traveling in CW are divided into two types based on their propagation directions, namely, the rightward propagation wave $f_R(x,t)$ and leftward propagation wave $f_L(x,t)$.

According to wave propagation theory, when the dispersion occurring at a high frequency is not considered, different wave propagation directions have the same frequency but can have different amplitudes and phases [38]. Therefore, the composite signal at Sensor 1 can be expressed as follows:

$$f_1(x_1,t) = A_R \cos(\omega t - kx_1 + \theta_R) + A_L \cos(\omega t + kx_1 + \theta_L), \quad (8)$$

in which

$$\begin{aligned}f_R(x_1,t) &= A_R \cos(\omega t - kx_1 + \theta_R) \\ f_L(x_1,t) &= A_L \cos(\omega t + kx_1 + \theta_L)\end{aligned}, \quad (9)$$

where k is the wavenumber and subscripts R and L are the rightward and leftward propagation waves, respectively.

The composite signal at Sensor 2 can be expressed in the same form:

$$\begin{aligned}f(x_2,t) &= A_R \cos(\omega t - kx_1 - k\Delta x + \theta_R) \\ &+ A_L \cos(\omega t + kx_1 + k\Delta x + \theta_L)\end{aligned}, \quad (10)$$

in which

$$x_2 = x_1 + \Delta x, \quad (11)$$

where Δx is the distance between the sensors.

Equations (8) and (10) are converted into the following forms based on the Euler's formula for derivation:

$$\eta(x_1,t) = A_R e^{i(\omega t - kx_1 + \theta_R)} + A_L e^{i(\omega t + kx_1 + \theta_L)} \quad (12)$$

$$\eta(x_2,t) = A_R e^{i(\omega t - kx_1 + \theta_R)} e^{-ik\Delta x} + A_L e^{i(\omega t + kx_1 + \theta_L)} e^{ik\Delta x}, \quad (13)$$

where $\eta(\bullet)$ is the plural transformation operator, i is the imaginary unit, and e is the Euler number. Then, the rightward and leftward propagation waves at Sensor 1 can be obtained by coupling Equations (12) and (13):

$$\eta_R(x_1,t) = A_R e^{i(\omega t - kx_1 + \theta_1)} = \frac{-\eta(x_1,t) e^{i \cdot k\Delta x} + \eta(x_2,t)}{-2i \sin(k\Delta x)} \quad (14)$$

$$\eta_L(x_1,t) = A_L e^{i(\omega t + kx_1 + \theta_1)} = \frac{\eta(x_1,t) e^{-ik\Delta x} - \eta(x_2,t)}{-2i \sin(k\Delta x)}. \quad (15)$$

The waves at Sensor 2 can also be obtained as follows:

$$\eta_R(x_2,t) = A_R e^{i(\omega t - kx_2 + \theta_R)} = \frac{-\eta(x_1,t) + \eta(x_2,t) e^{-ik\Delta x}}{-2i \sin(k\Delta x)} \quad (16)$$

$$\eta_L(x_2,t) = A_L e^{i(\omega t + kx_2 + \theta_L)} = \frac{\eta(x_1,t) - \eta(x_2,t) e^{i \cdot k\Delta x}}{-2i \sin(k\Delta x)}. \quad (17)$$

Note that the signal $f(x,t)$ obtained using the sensors is the real part of $\eta(x,t)$. The Hilbert transform is adopted to define the relation between the obtained and analytical signals to ensure that the presented decomposition process is applicable to the single CW test signal.

$$\eta(t) = f(t) + i\mathbf{H}[f(t)], \quad (18)$$

where $\mathbf{H}(\bullet)$ is the Hilbert operator.

For Sensor 1, the rightward incident wave at t_0 is denoted as $f_R(x_1,t_0)$. Then, the reflection coefficient r_m can be directly obtained as

$$r_m = 1 - \frac{f_R(x_2, t_0 + \Delta t)}{f_R(x_1, t_0)}, \quad (19)$$

in which

$$\Delta t = \frac{\Delta x}{v},$$

where Δt is the travel time from Sensor 1 to Sensor 2, v is the wave speed at a certain frequency, and $f_R(x_2, t_0 + \Delta t)$ is the rightward propagation wave obtained using Sensor 2 at $t_0 + \Delta t$. Based on the aforementioned derivations, the decomposition process of the composite signal in the CW tests can be described as shown in Fig. 9.

In Fig. 7(b), the acceleration spectrum has three dominant frequencies that represent the first three natural frequencies of the single CW. The waves with these three frequencies are decomposed to extract the incident and reflection waves using the aforementioned decomposition process. According to Equations (14)–(18), the rightward and leftward propagation waves with a certain frequency obtained using Sensors 1 and 2 are presented in Fig. 10.
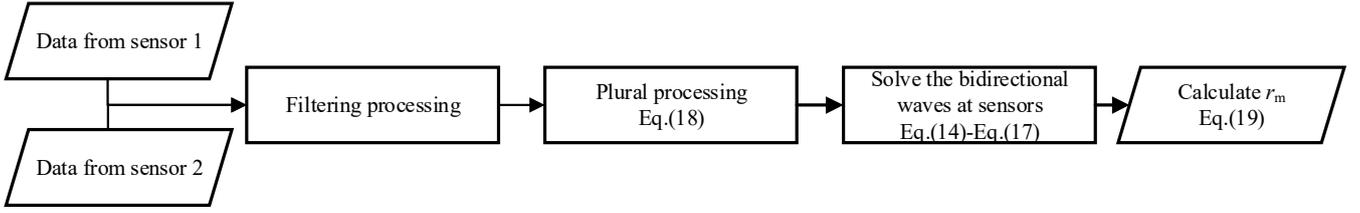
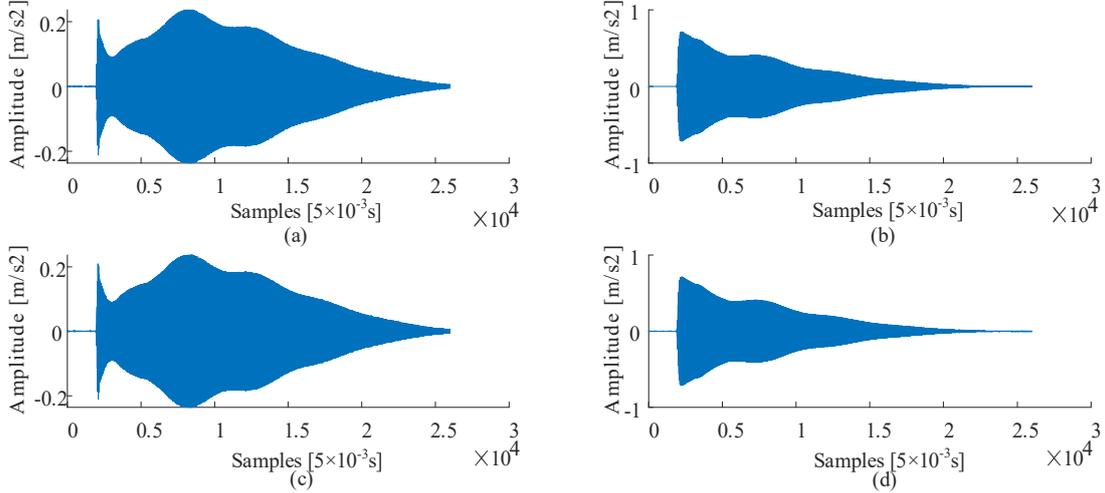Fig. 9 Decomposition process of the composite signal in the CW test.

Fig. 10 Wave components with the first-order frequency. (a) Rightward propagation wave at Sensor 1. (b) Leftward propagation wave at Sensor 1. (c) Rightward propagation wave at Sensor 2. (d) Leftward propagation wave at Sensor 2.
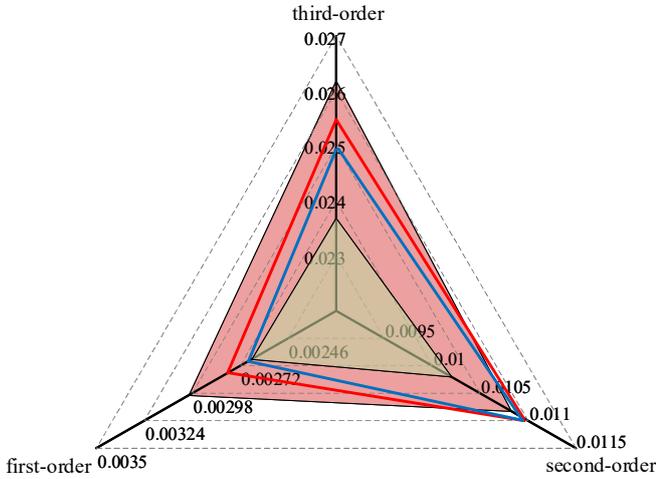
Fig. 11 Reflection coefficients of the single CW with 13-kN and 15-kN tensions. Pink area: reflection coefficient with 13-kN tension. Oliver area: reflection coefficient with 15-kN tension. Red solid line: theoretical results with 13-kN tension. Blue solid line: theoretical results with 15-kN tension.
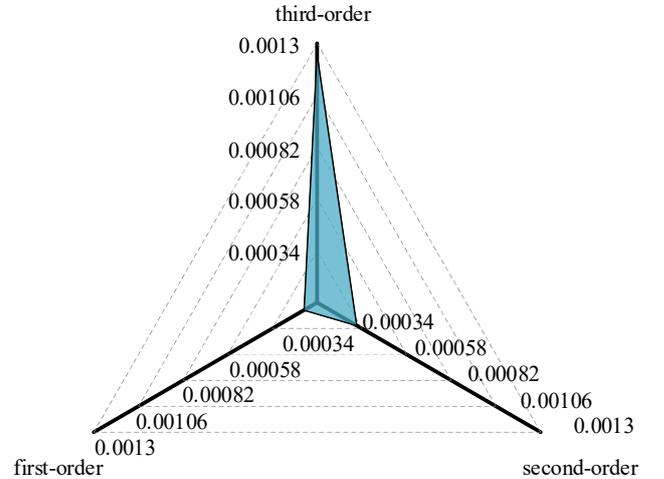
Fig. 12 Reflection coefficient ratios versus tension.

The classical definition of the reflection coefficient in the single cable with attached mass is given as Equation (20):

$$r = \frac{-\mu\omega(i + \mu\omega)}{1 + \mu^2\omega^2}, \quad \mu = m/(2\rho v), \tag{20}$$

where m is the weight of mass, ρ and v denote the cable linear density and the wave speed, respectively. ω is the wave angular frequency and i is the imaginary unit. Then it is easy to obtain the theoretical reflection coefficients of the single CW

at different frequencies with the collected parameters in Table II.

Fig. 11 demonstrates the comparison of reflection coefficients between the theoretical results and the test results. It is reported that a larger tension in the CW leads to a smaller reflection coefficient. And it is also indicated by Fig. 11 that, although there are some differences between the theoretical results and the test results, the errors are all acceptable with the values being kept below 10%. Fig. 12 presents the ratios of the differences in the reflection coefficient versus the differences in
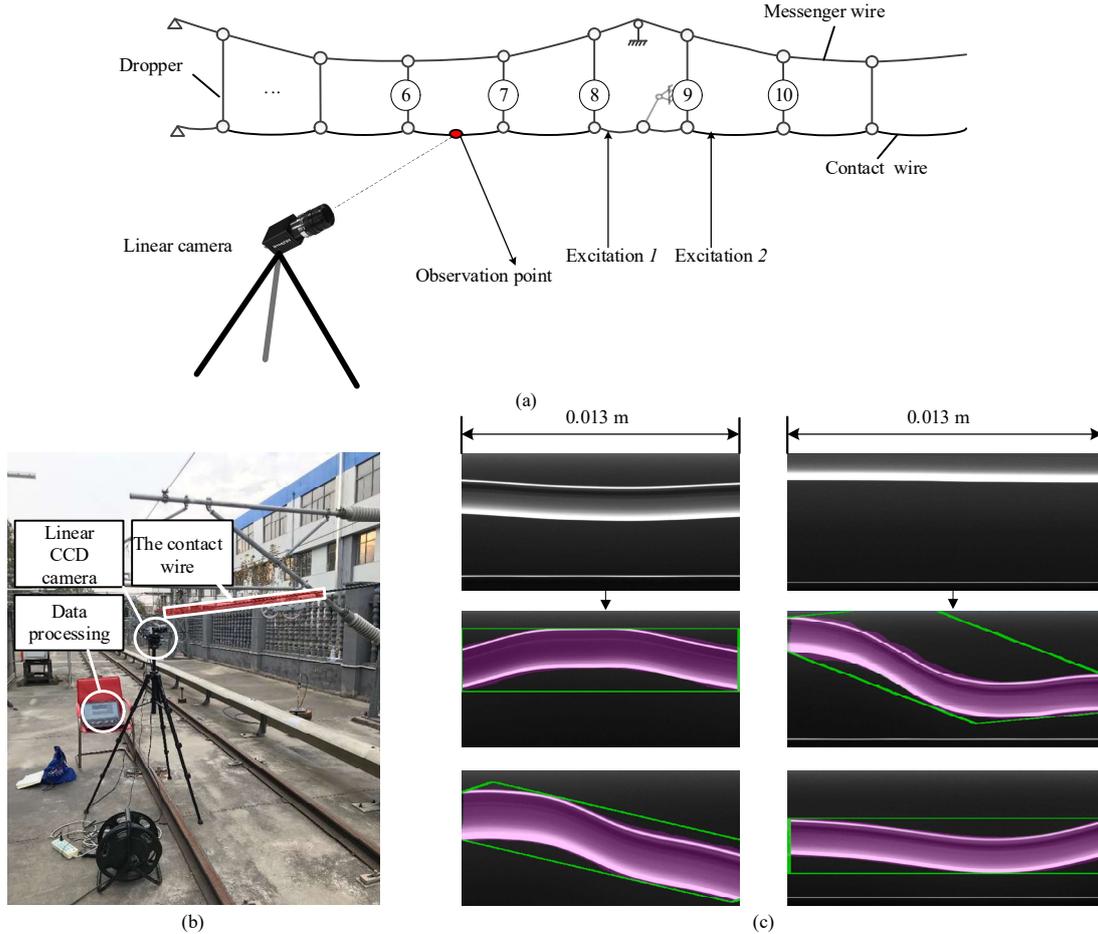
Fig. 13 (a) Schematic of full-scale catenary uplift detection. (b) Photogrammetric devices and test catenary line. (c) Identification results of the contact wire.

the tension. The results indicate that the reflection coefficient related to the higher-order frequency is more sensitive to changes in tension. However, even for CW with 15-kN tension, the reflection coefficients related to the main frequencies are lower than 0.03. We conclude that the lumped mass is not the leading cause of the wave reflection. It is necessary to investigate the wave reflection occurring at a real-life dropper junction in a full-scale catenary.

IV. ANALYSIS OF WAVE REFLECTION IN FULL-SCALE CATENARY

Previous studies have shown that the wave reflection occurring at the dropper junction has a distinct impact on the pantograph–catenary interaction [35][37]. In Section III, the single CW test results indicate that the mass discontinuity caused by the dropper mass is not the main factor inducing wave reflection. For a full-scale catenary structure, which is different from the single CW, the wave is reflected and diffracted at the dropper clamp as well as transmitted upward along MW and back to CW through the dropper connection. Therefore, an experimental test is conducted on a full-scale catenary to investigate the complex wave propagation behavior in this section. Further, an advanced analytical approach is provided to extract wave components in different propagation stages.

TABLE III
PARAMETERS OF THE TESTED CATENARY LINE

Parameter	Value
Tension force of the contact wire	15 kN
Tension force of the messenger wire	13 kN
Interval of adjacent droppers	6.5 m
Linear density of the contact wire	1.3350 kg/m
Linear density of the messenger wire	1.0680 kg/m

A. Test setup of full-scale catenary

The noncontact measurement approach is adopted to obtain the catenary dynamic response and reduce the disturbance of the contact sensors in the measurement results. The measurement equipment was developed in our previous work based on photogrammetry [31] (Fig. 13(a)). In this study, CW vibration images are captured using a high-speed linear camera with an acquisition frequency of 50 FPS. The photogrammetric devices and identification results of CW are presented in Fig. 13(b and c), and some of the catenary parameters listed in Table III. In this study, the observation position is set at the midpoint between Droppers 6 and 7. Then, CW is lifted at a certain height to apply impulse excitation near Droppers 8 and 9. The measurement results of the CW uplift are shown in Fig. 14, along with their spectra. For the full-scale catenary tests in this
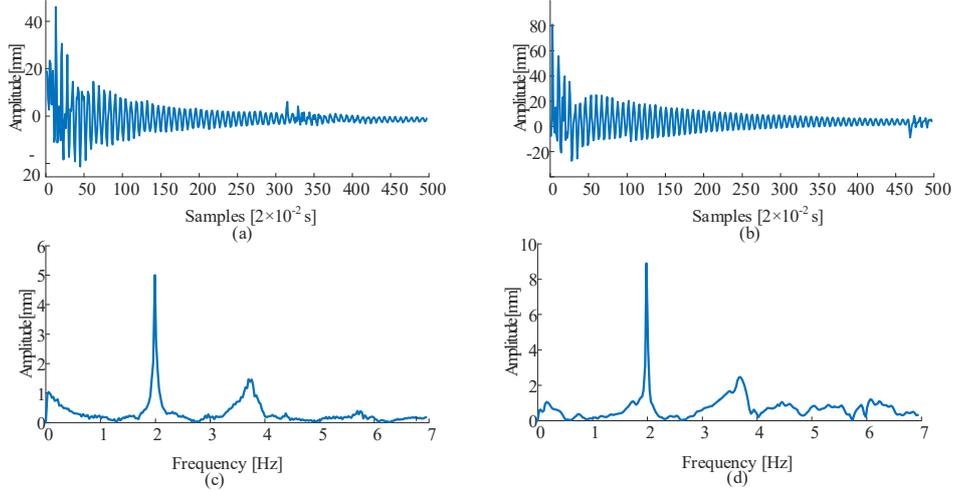
Fig. 14 Dynamic uplift of the contact wire. (a) Excitation at Dropper 9. (b) Excitation at Dropper 8. (c) Frequencies of (a). (d) Frequencies of (b).
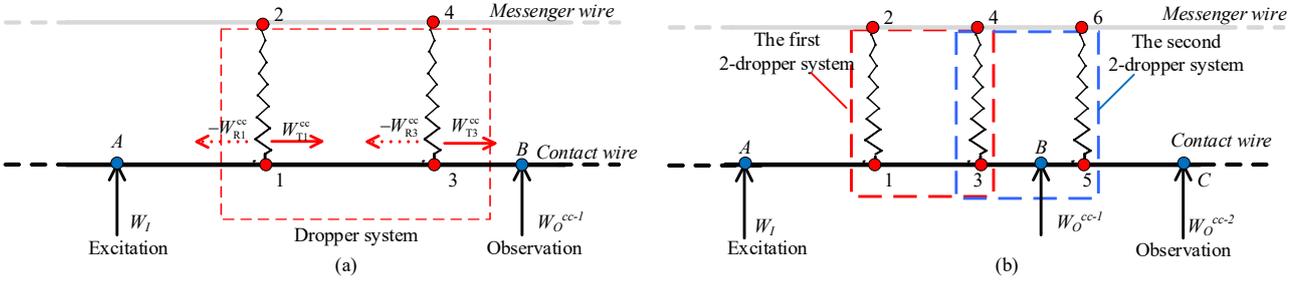
Fig. 15 Simplified model considering droppers hanging on CW. (a) Simplified contact wire with double droppers. (b) Simplified contact wire with three droppers.
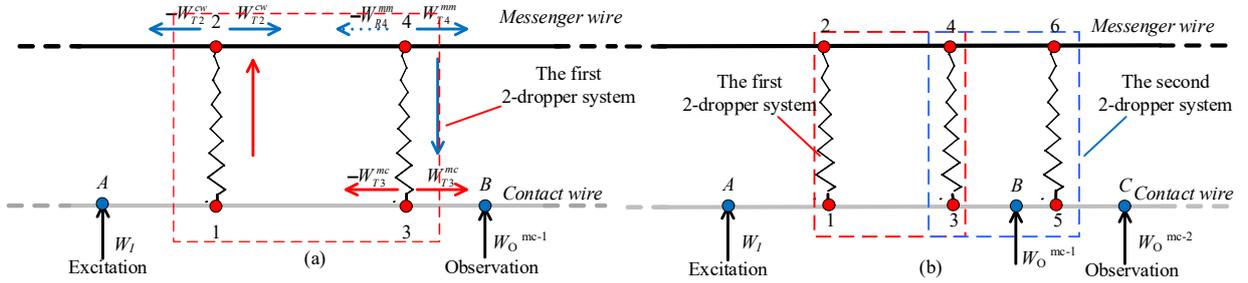
Fig. 16 Simplified catenary with waves transmitting from MW. (a) Simplified model with a single two-dropper system. (b) Simplified model with double two-dropper systems.

paper, only the waves with the first-order frequency are considered as the wave energy is mostly centered therein.

B. Analytical approach to identifying the reflection coefficient

As the effect of wave propagation in MW has a negligible effect on the reflection in CW (Section II), the simplified model in Fig. 15(a), which contains one CW and two droppers, is used

The two droppers and one CW produce a wave reflective cavity, in which multiple wave reflections and transmissions occur. Therefore, the composite wave obtained at Point B can be divided into two parts: (1) the wave component directly transmitted through the cavity without any reflection and follows the propagation path A → 1 → 3 → B and (2) the wave component generated by multiple reflections in the cavity and follows the propagation path A → 1 → 3 → 1 →…→ 3 → B.

Assuming that the droppers exhibit the same reflection property and the change in the phase is negligible, W_O^{cc-1} in Fig.

to analyze the wave propagation. The uplift excitation is applied to Point A, which induces traveling wave W_I in CW. Then, the wave is reflected and transmitted at every dropper joint. As shown in Fig. 15(a), the reflection and transmission waves are denoted by W_{R1}^{cc}, W_{R3}^{cc}, W_{T1}^{cc} and W_{T3}^{cc}, respectively.

15(a) can be expressed as follows:

$$W_O^{cc-1} = W_I^0 + W_I^1 + ... + W_I^n, \tag{21}$$

in which

$$\begin{cases} W_I^0 = W_I \cdot \left(1 - r_d^{cw}\right)^2 \cdot \left(r_d^{cw}\right)^0 \\ W_I^1 = W_I \cdot \left(1 - r_d^{cw}\right)^2 \cdot \left(r_d^{cw}\right)^2 \quad , n = 0,1,2,3... \\ W_I^n = W_I \cdot \left(1 - r_d^{cw}\right)^2 \cdot \left(r_d^{cw}\right)^{2n} \end{cases} \tag{22}$$

where n is the number of reflections in the cavity between the

two droppers. Then, Equation (21) can be simplified to

$$W_{\mathrm{O}}^{\mathrm{cc-1}} = W_{\mathrm{I}}\left(1-r_{\mathrm{d}}^{\mathrm{cw}}\right)^2 \sum_n \left(r_{\mathrm{d}}^{\mathrm{cw}}\right)^{2n}. \tag{23}$$

Based on this concept, more complex structures can be analyzed. The CW with three droppers is presented in Fig. 15(b), where two reflection cavities are formed. Each cavity comprises two adjacent droppers. According to Equations (21) and (22), the observation wave in Fig. 15(b) can be expressed as follows:

$$\begin{aligned} W_{\mathrm{O}}^{\mathrm{cc-2}} &= W_{\mathrm{I}} \cdot \left(1-r_{\mathrm{d}}^{\mathrm{cw}}\right)^3 \sum_n \left(r_{\mathrm{d}}^{\mathrm{cw}}\right)^{2n} \sum_m \left(r_{\mathrm{d}}^{\mathrm{cw}}\right)^{2m} \\ &= W_{\mathrm{O}}^{\mathrm{cc-1}} \cdot \left(1-r_{\mathrm{d}}^{\mathrm{cw}}\right) \sum_m \left(r_{\mathrm{d}}^{\mathrm{cw}}\right)^{2m} \end{aligned}, \tag{24}$$

$$n = 0,1,2,3,\dots, m = 0,1,2,3,\dots$$

where n and m are the reflection numbers in the first and second cavities, respectively.

Two models are established by considering the waves traveling in MW (Fig. 16). The waves are transmitted upward from CW to MW and then back to CW through the dropper connection. Based on this approach, the composite wave $W_{\mathrm{O}}^{\mathrm{mc-1}}$ in Fig. 16(a) can be divided into two parts: (1) $W_{1\text{-}1}^{\mathrm{mc}}$ —the wave components directly transmitted from MW and follow the propagation path $A \to 1 \to 2 \to 4 \to 2 \to \dots \to 4 \to 3 \to B$ and (2) $W_{1\text{-}2}^{\mathrm{mc}}$ —the wave components generated by the multiple reflections of $W_{1\text{-}1}^{\mathrm{mc}}$ in CW and follow the propagation path $A \to 1 \to 2 \to \dots \to 4 \to 3 \to 1 \to \dots \to 3 \to B$.

Then, the composite signal in Fig. 16(a) can be expressed as follows:

$$W_{\mathrm{O}}^{\mathrm{mc-1}} = W_{1\text{-}1}^{\mathrm{mc}} + W_{1\text{-}2}^{\mathrm{mc}}, \tag{25}$$

in which

$$W_{1\text{-}1}^{\mathrm{mc}} = W_{\mathrm{I}}\left(1-r_{\mathrm{d}}^{\mathrm{cw}}\right)\left(1-r_{\mathrm{d}}^{\mathrm{mw}}\right) \sum_j \left(r_{\mathrm{d}}^{\mathrm{mw}}\right)^{2j}$$

$$W_{1\text{-}2}^{\mathrm{mc}} = W_{\mathrm{I}}\left(1-r_{\mathrm{d}}^{\mathrm{cw}}\right)^2\left(1-r_{\mathrm{d}}^{\mathrm{mw}}\right) \sum_j \left(r_{\mathrm{d}}^{\mathrm{mw}}\right)^{2j} \cdot \sum_k \left(r_{\mathrm{d}}^{\mathrm{cw}}\right)^{2k-1}, \tag{26}$$

$$j = 0,1,2,3,\dots, \ k = 1,2,3,\dots$$

where j and k are the number of reflections in the cavity between two droppers in MW and CW, respectively.

For the model shown in Fig. 16(b), the composite signal $W_{\mathrm{O}}^{\mathrm{mc-2}}$ can also be divided into two parts:

$$W_{\mathrm{O}}^{\mathrm{mc-2}} = W_{2\text{-}1}^{\mathrm{mc}} + W_{2\text{-}2}^{\mathrm{mc}} \tag{27}$$

$$W_{2\text{-}1}^{\mathrm{mc}} = W_{\mathrm{O}}^{\mathrm{mc-1}} \cdot \left(1-r_{\mathrm{d}}^{\mathrm{cw}}\right) \cdot \sum_p \left(r_{\mathrm{d}}^{\mathrm{cw}}\right)^{2p}$$

$$W_{2\text{-}2}^{\mathrm{mc}} = W_{\mathrm{I}}\left(1-r_{\mathrm{d}}^{\mathrm{cw}}\right)\left(1-r_{\mathrm{d}}^{\mathrm{mw}}\right)^2 \cdot \sum_j \left(r_{\mathrm{d}}^{\mathrm{mw}}\right)^{2j} \cdot \sum_q \left(r_{\mathrm{d}}^{\mathrm{mw}}\right)^{2q}, \tag{28}$$

$$p = 0,1,2,3,\dots \ q = 0,1,2,3,\dots$$

where p and q are the number of reflections in the second cavity in MW and CW, respectively.

Therefore, the composite signals of the two models can be expressed as follows:

$$\begin{aligned} W_{\mathrm{O}}^1 &= W_{\mathrm{O}}^{\mathrm{mc-1}} + W_{\mathrm{O}}^{\mathrm{cc-1}} \\ W_{\mathrm{O}}^2 &= W_{\mathrm{O}}^{\mathrm{mc-2}} + W_{\mathrm{O}}^{\mathrm{cc-2}}, \end{aligned} \tag{29}$$

where superscripts 1 and 2 denote the number of the two-dropper system in the model.

Because the droppers exhibit the same reflection properties, the wave will reflect in similar orders in both the two-dropper systems. Considering that the reflection coefficients of the catenary structure are always less than 0.5 [39], in this study, the maximal order of reflection in the two-dropper system is limited to 4, wherein the wave components that decay to less than 5% of the initial value are negligible. Then, Equation (29) can be rewritten using a given order of reflection β.

$$\begin{aligned} W_{\mathrm{O}}^1 &= W_{\mathrm{O}}^{\mathrm{mc-1}} + W_{\mathrm{O}}^{\mathrm{cc-1}} \\ &= W_{\mathrm{I}}\left(1-r_{\mathrm{d}}^{\mathrm{cw}}\right)\left(1-r_{\mathrm{d}}^{\mathrm{mw}}\right) \sum_\xi \left(r_{\mathrm{d}}^{\mathrm{mw}}\right)^{2\beta} \left[1 + \left(1-r_{\mathrm{d}}^{\mathrm{cw}}\right) \sum_\xi \left(r_{\mathrm{d}}^{\mathrm{cw}}\right)^{2\beta-1}\right] \\ &\quad + W_{I}\left(1-r_{d}^{\mathrm{cw}}\right)^2 \sum_\beta \left(r_{d}^{\mathrm{cw}}\right)^{2\beta} \end{aligned}$$

$$\begin{aligned} W_{\mathrm{O}}^2 &= W_{\mathrm{O}}^{\mathrm{mc-2}} + W_{\mathrm{O}}^{\mathrm{cc-2}} \\ &= f_{\mathrm{mc}}\left(W_{\mathrm{O}}^{\mathrm{mc-1}}\right) + f_{\mathrm{cc}}\left(W_{\mathrm{O}}^{\mathrm{cc-1}}\right) \end{aligned}$$

$$\beta = 0,1,2,3,4, \tag{30}$$

in which

$$f_{\mathrm{mc}}\left(W_{\mathrm{O}}^{\mathrm{mc-1}}\right) = W_{\mathrm{O}}^{\mathrm{mc-1}}\left(1-r_{\mathrm{d}}^{\mathrm{cw}}\right) \sum_\beta \left(r_{\mathrm{d}}^{\mathrm{cw}}\right)^{2\beta}$$

$$f_{\mathrm{cc}}\left(W_{\mathrm{O}}^{\mathrm{cc-1}}\right) = W_{\mathrm{O}}^{\mathrm{cc-1}}\left[\left(1-r_{\mathrm{d}}^{\mathrm{cw}}\right) \sum_\beta \left(r_{\mathrm{d}}^{\mathrm{cw}}\right)^{2\beta} + \frac{\left(1-r_{\mathrm{d}}^{\mathrm{mw}}\right)^2 \sum_\beta \left(r_{\mathrm{d}}^{\mathrm{mw}}\right)^{2\beta}}{\left(1-r_{\mathrm{d}}^{\mathrm{cw}}\right)}\right]$$

where $f_{\mathrm{mc}}(\bullet)$ and $f_{\mathrm{cc}}(\bullet)$ are the two self-defined functions to simplify Equation (30).

For Equation (30), the wave components arriving at the observation site at different times can be obtained using different β values. Note that the time differences between the wave components are mainly caused by the differences in the traveling speed and distance of the waves. The speed of the wave traveling in CW and MW is denoted as v_{cw} and v_{mw}, respectively, which can be calculated using their tensions and linear densities [40]. The interval between the two adjacent droppers is defined as l_{d}. Then, the time delay caused by the reflection in one cavity can be expressed as follows:

$$\begin{aligned} \Delta t_{\mathrm{cw}} &= l_{\mathrm{d}} / v_{\mathrm{cw}} \\ \Delta t_{\mathrm{mw}} &= l_{\mathrm{d}} / v_{\mathrm{mw}}, \end{aligned} \tag{31}$$

where Δt_{cw} and Δt_{mw} are the time delays occurring in CW and MW, respectively.

Considering the plural form of the waves with time delay, Equation (30) can be rewritten as follows:

$$\begin{aligned} \eta\left(W_{\mathrm{O}}^1\right) &= \eta\left(W_{\mathrm{O}}^{\mathrm{mc-1}}\right) + \eta\left(W_{\mathrm{O}}^{\mathrm{cc-1}}\right) \\ \eta\left(W_{\mathrm{O}}^2\right) &= \eta\left[f_{\mathrm{mc}}\left(W_{\mathrm{O}}^{\mathrm{mc-2}}\right)\right] + \eta\left[f_{\mathrm{cc}}\left(W_{\mathrm{O}}^{\mathrm{cc-2}}\right)\right], \end{aligned} \tag{32}$$

in which

$$\eta\left(W_{\mathrm{O}}^{\mathrm{mc\text{-}1}}\right)=\eta\left(W_{\mathrm{I}}\right)\left(1-r_{\mathrm{d}}^{\mathrm{cw}}\right)\left(1-r_{\mathrm{d}}^{\mathrm{mw}}\right)\sum_{\xi}\left(r_{\mathrm{d}}^{\mathrm{mw}}\right)^{2\xi}\cdots$$

$$\cdots\left[1+\left(1-r_{\mathrm{d}}^{\mathrm{cw}}\right)\sum_{\xi}\left(r_{\mathrm{d}}^{\mathrm{cw}}\right)^{2\xi-1}\cdot e^{-i\omega(2\xi-1)\Delta t_{\mathrm{cw}}}\right]e^{-i\omega(2\xi+1)\Delta t_{\mathrm{mw}}}$$

$$\eta\left(W_{\mathrm{O}}^{\mathrm{cc\text{-}1}}\right)=\eta\left(W_{\mathrm{I}}\right)\left(1-r_{\mathrm{d}}^{\mathrm{cw}}\right)^{2}\sum_{\xi}\left(r_{\mathrm{d}}^{\mathrm{cw}}\right)^{2\xi}e^{-i\omega(2\xi+1)\Delta t_{\mathrm{cw}}}$$

$$\eta\left[f_{\mathrm{mc}}\left(W_{\mathrm{O}}^{\mathrm{mc\text{-}1}}\right)\right]=\eta\left(W_{\mathrm{O}}^{\mathrm{mc\text{-}1}}\right)\cdot\left(1-r_{\mathrm{d}}^{\mathrm{cw}}\right)\sum_{\xi}\left(r_{\mathrm{d}}^{\mathrm{cw}}\right)^{2\xi}e^{-i\omega(2\xi)\Delta t_{\mathrm{cw}}}$$

$$\eta\left[f_{\mathrm{cc}}\left(W_{\mathrm{O}}^{\mathrm{cc\text{-}1}}\right)\right]=\eta\left(W_{\mathrm{O}}^{\mathrm{cc\text{-}1}}\right)\left(1-r_{\mathrm{d}}^{\mathrm{cw}}\right)\sum_{\xi}\left(r_{\mathrm{d}}^{\mathrm{cw}}\right)^{2\xi}e^{-i\omega(2\xi+1)\Delta t_{\mathrm{cw}}}$$

$$+\eta\left(W_{\mathrm{O}}^{\mathrm{cc\text{-}1}}\right)\frac{\left(1-r_{\mathrm{d}}^{\mathrm{mw}}\right)^{2}\sum_{\xi}\left(r_{\mathrm{d}}^{\mathrm{mw}}\right)^{2\xi}e^{-i\omega(2\xi+1)\Delta t_{\mathrm{mw}}}}{\left(1-r_{\mathrm{d}}^{\mathrm{cw}}\right)}$$

where ω is the wave angular frequency and $\eta(\bullet)$ is the operator shown in Equation (18).

C. Analysis results of wave reflection in catenary

As the energy of the obtained waves is mainly centered in the low-order frequencies (Fig. 14), only waves with first-order frequencies are extracted in this study. Based on the measured tension forces and linear densities, the traveling speed of the wave in CW is nearly similar to that in MW, thus yielding approximately similar time decays in the two wires, i.e., $\Delta t_{\mathrm{cw}}\approx\Delta t_{\mathrm{mw}}$.

1) Reflection coefficients of the catenary structure

For the catenary whose structural parameters are not available, extracting the actual reflection coefficient from the measured data can help evaluate the contact quality between the pantograph and catenary at the theoretical level.

According to Equations (30)–(32), the reflection coefficient of the catenary can be obtained by plugging in the reflection order and observation wave. Fig. 17 shows the comparisons of the reflection coefficient in CW between the results obtained from the field tests and theoretical results. When the back-and-forth reflections are ignored, i.e., the reflection order is set to 0, the reflection coefficient obtained from the measured data and the theoretical results differs by more than 50%. As the reflection order increases, the error tends to decrease, particularly when the value is set to greater than 3. The difference can be retained below 5%.

2) Wave components at the observation site

Extracting the wave components from the actual measured data is meaningful for future research on wave propagation characteristics in the catenary structure. For the catenary whose design reflection coefficient is available, the proposed analytical method provides a feasible approach for decomposing the composite signal into wave components with different reflection orders.

According to Equations (30)–(32), the wave components at the observation site can be obtained by setting the reflection order β to different values when plugging in the design reflection coefficients and given incident wave. Based on the single CW test, the attached masses have an inconsiderable influence on the wave reflection. Thus, the imaginary parts
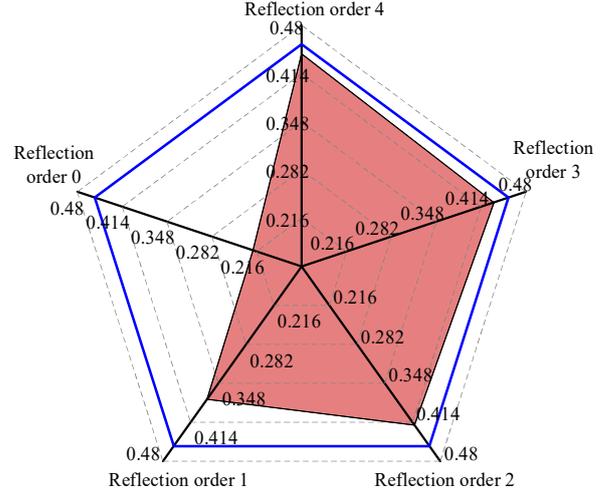

Fig. 17 Reflection coefficients with different reflection orders. Pink area: reflection coefficients obtained from the field test. Blue solid line: the theoretical value of the reflection coefficient.
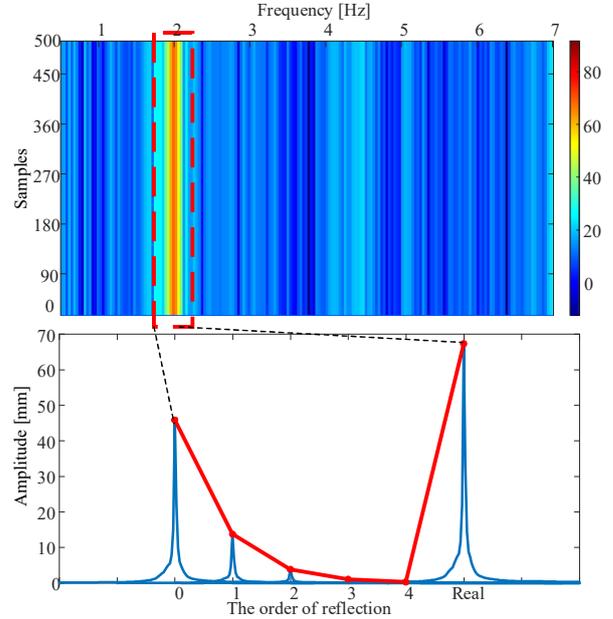

Fig. 18 Signal extraction and intensities of the wave components.

related to the clamp masses can be ignored when calculating the lower-frequency wave propagation, as shown in Equation (33):

$$r_{\mathrm{d}}^{\mathrm{cw}}=\frac{\sqrt{S_{\mathrm{mw}}\rho_{\mathrm{mw}}}}{\sqrt{S_{\mathrm{mw}}\rho_{\mathrm{mw}}}+\sqrt{S_{\mathrm{cw}}\rho_{\mathrm{cw}}}}$$
$$r_{\mathrm{d}}^{\mathrm{mw}}=\frac{\sqrt{S_{\mathrm{cw}}\rho_{\mathrm{mw}}}}{\sqrt{S_{\mathrm{mw}}\rho_{\mathrm{mw}}}+\sqrt{S_{\mathrm{cw}}\rho_{\mathrm{cw}}}} \quad (33)$$

Fig. 18 shows the signal intensities of the wave components obtained using the proposed analytical method, all with first-order frequencies, as shown in the spectrum result. The composite signal energy is mainly centered in the wave component without the back-and-forth reflections. When the reflection order increases, the intensity of the wave component rapidly decreases. When the reflection order is set to greater than 3, the wave component intensity decreases to a lower level
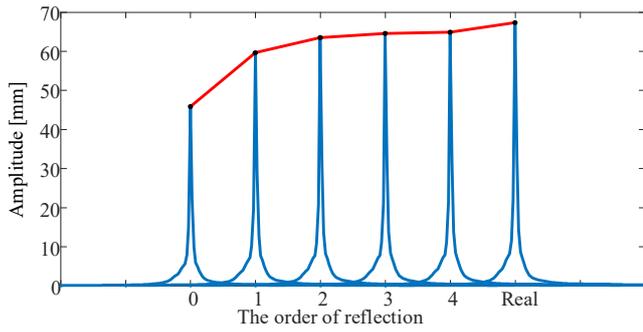
Fig. 19 Intensities of the composite signal obtained using different reflection orders.

that is negligible for the catenary vibration analysis. Fig. 19 presents the composite signal obtained using different reflection orders. Obviously, when the reflection order is set to greater than 3, the calculated results are approximately close to the measured results.

V. CONCLUSIONS

A catenary is a specific type of waveguide structure comprising two overhead cables connected by droppers. Waveguide discontinuities at the dropper junctions induce wave reflection, making the waves traveling in the catenary structure to behave more intricately. The catenary reflection coefficient at the dropper junction is an important index for assessing the contact performance between the pantograph and CW. However, obtaining the actual reflection coefficient of the catenary based on field measurements is challenging.

In this study, two kinds of field measurements were conducted to obtain the dynamic responses of the single CW and full-scale catenary, respectively. On the basis of the measured data, a novel analytical approach is proposed to identify the catenary structure's actual reflection coefficient based on field measurements. The results in the single CW tests, which are designed to simulate wave reflection caused by the mass discontinuity, are justified effective in identifying the wave reflection coefficients with an acceptable error. It is also suggested that the dropper clamp has an insignificant influence on wave reflection, and the reflection coefficients related to the higher frequencies have more sensitivity to tension change. In the full-scale catenary test, the reassembled models are applied to separate the catenary wave propagation into the CW–CW part and CW–MW part, based on which analytical models of wave reflection at droppers are formulated. The analytical models were proven effective for reflection coefficient identification of the catenary and wave component extraction based on the measured data. The results also suggest that the back-and-forth reflection occurring in the adjacent droppers has a noticeable impact on wave propagation.

In conclusion, this paper proposes an effective approach for reflection coefficient identification and wave components extraction in the railway catenary structure. The results can help reveal the wave propagation characteristics of the catenary system in future work and improve pantograph–catenary interaction by restraining wave reflection of the catenary

structure.

REFERENCES

[1] M. Dehestani, M. Mofid, and A. Vafai, "Investigation of critical influential speed for moving mass problems on beams," *Appl. Math. Model*, vol. 33, no. 10, pp. 3885–3895, Oct. 2009.

[2] J. R. Rieker, Y. H. Lin, and M. W. Trethewey, "Discretization considerations in moving load finite element beam models," *Finite Elem. Anal. Des.*, vol. 21, no. 3, pp. 129–144, 1996.

[3] J. R. Rieker and M. W. Trethewey, "Finite element analysis of an elastic beam structure subjected to a moving distributed mass train," *Mech. Syst. Signal Process*, vol. 13, no. 1, pp. 31–51, 1999.

[4] U. Lee, "Separation between the flexible structure and the moving mass sliding on it," *J. Sound Vib.*, vol. 209, no. 5, pp. 867–877, 1998.

[5] D. Stancioiu, H. Ouyang, and J. E. Mottershead, "Dynamics of a beam and a moving two-axle system with separation," *Proc. Inst. Mech. Eng. C. J. Mech. Eng. Sci.*, vol. 222, no. 10, pp. 1947–1956, 2008.

[6] K. Lee, Y. Cho, and J. Chung, "Dynamic contact analysis of a tensioned beam with a moving mass–spring system," *J. Sound Vib.*, vol. 331, no. 11, pp. 2520–2531, 2012.

[7] S. Gregori, M. Tur, A. Pedrosa, J. E. Tarancón, and F. J. Fuenmayor, "A modal coordinate catenary model for the real-time simulation of the pantograph–catenary dynamic interaction," *Finite Elem. Anal. Des.*, vol. 162, pp. 1–12, 2019.

[8] M. Tur, E. García, L. Baeza, and F. J. Fuenmayor, "A 3D absolute nodal coordinate finite element model to compute the initial configuration of a railway catenary," *Eng. Struct.*, vol. 71, pp. 234–243, 2014.

[9] Y. Song, Z. Liu, Z. Xu, and J. Zhang, "Developed moving mesh method for high-speed railway pantograph–catenary interaction based on nonlinear finite element procedure," *Int. J. Rail Transp.*, vol. 7, no. 3, pp. 173–190, 2019.

[10] E. Arias *et al.*, "A mathematical model of the static pantograph/catenary interaction," *Int. J. Comput. Math.*, vol. 86, no. 2, pp. 333–340, 2009.

[11] J. Ambrósio, F. Rauter, J. Pombo, and M. Pereira, "Dynamics of high-speed train pantograph–catenary co-simulation of finite element and multibody codes" *AIP Conf. Proc.*, vol. 1233, no. 1, pp. 213–218, 2010.

[12] Y. Song, Z. Liu, H. Wang, X. Lu, and J. Zhang, "Nonlinear modelling of high-speed catenary based on analytical expressions of cable and truss elements," *Veh. Syst. Dyn.*, vol. 53, no. 10, pp. 1455–1479, 2015.

[13] Y. Song, Z. Liu, H. Wang, X. Lu, and J. Zhang, "Nonlinear analysis of wind-induced vibration of high-speed railway catenary and its influence on pantograph–catenary interaction," *Veh. Syst. Dyn.*, vol. 54, no. 6, pp. 723–747, 2016.

[14] M. T. Stickland and T. J. Scanlon, "An investigation into the aerodynamic characteristics of catenary contact wires in a cross-wind," *Proc. Inst. Mech. Eng. F. J. Rail Rapid Transit*, vol. 215, no. 4, pp. 311–318, 2001.

[15] A. Carnicero, J. R. Jimenez-Octavio, C. Sanchez-Rebollo, A. Ramos, and M. Such, "Influence of track irregularities in the catenary–pantograph dynamic interaction," *J. Comput. Nonlinear Dyn.*, vol. 7, no. 4, 2012, Art. no. 041015.

[16] Y. Song, Z. Wang, Z. Liu, and R. Wang, "A spatial coupling model to study dynamic performance of pantograph-catenary with vehicle-track excitation," *Mech. Syst. Signal Process,* vol. 151, p. 107336, 2020.

[17] H. Wang *et al.*, "Detection of contact wire irregularities using a quadratic time–frequency representation of the pantograph–catenary contact force," *IEEE Trans. Instrum. Meas.*, vol. 65, no. 6, pp. 1385–1397, 2016.

[18] Y. Song, Z. Liu, and X. Lu, "Dynamic performance of high-speed railway overhead contact line interacting with pantograph considering local dropper defect," *IEEE Trans. Veh. Technol.*, vol. 69, no. 6, pp. 5958–5967, 2020.

[19] Y. Song, Z. Liu, A. Rønnquist, P. Nåvik, and Z. Liu, "Contact wire irregularity stochastics and effect on high-speed railway pantograph–catenary interactions," *IEEE Trans. Instrum. Meas.*, vol. 69, no. 10, pp. 8196–8206, Oct. 2020, doi: 10.1109/TIM.2020.2987457.

[20] P. Nåvik, A. Rønnquist, and S. Stichel, "Identification of system damping in railway catenary wire systems from full-scale measurements," *Eng. Struct.*, vol. 113, pp. 71–78, 2016.

[21] J. Chen, Z. Liu, H. Wang, A. Núñez, and Z. Han, "Automatic defect detection of fasteners on the catenary support device using deep convolutional neural network," *IEEE Trans. Instrum. Meas.*, vol. 67, no. 2, pp. 257–269, 2017.

[22] H. Wang, A. Núñez, Z. Liu, Y. Song, F. Duan, and R. Dollevoet, "Analysis of the evolvement of contact wire wear irregularity in railway

catenary based on historical data," *Veh. Syst. Dyn.*, vol. 56, no. 8, pp. 1207–1232, 2018.

[23] H. Wang, Z. Liu, A. Núñez, and R. Dollevoet, "Entropy-based local irregularity detection for high-speed railway catenaries with frequent inspections," *IEEE Trans. Instrum. Meas.*, vol. 68, no. 10, pp. 3536–3547, 2018.

[24] Z. Xu, Y. Song, and Z. Liu, "Effective measures to improve current collection quality for double pantographs and catenary based on wave propagation analysis," *IEEE Trans. Veh. Technol.*, vol. 69, no. 6, pp. 6299–6309, Jun. 2020, doi: 10.1109/TVT.2020.2985382.

[25] Y. H. Cho, "Numerical simulation of the dynamic responses of railway overhead contact lines to a moving pantograph, considering a nonlinear dropper," *J. Sound Vib.*, vol. 315, no. 3, pp. 433–454, 2008.

[26] K. Schröder, W. Ecke, M. Kautz, S. Willett, M. Jenzer, and T. Bosselmann, "An approach to continuous on-site monitoring of contact forces in current collectors by a fiber optic sensing system," *Opt. Lasers Eng.*, vol. 51, no. 2, pp. 172-179, 2013.

[27] H. Wang, Z. Liu, A. Núñez, and R. Dollevoet, "Identification of the catenary structure wavelength using pantograph head acceleration measurements," in *2017 IEEE International Instrumentation and Measurement Technology Conference (I2MTC)*, 2017, pp. 1-6: IEEE.

[28] D. Zou, W. H. Zhang, R. P. Li, N. Zhou, and G. M. Mei, "Determining damping characteristics of railway-overhead-wire system for finite-element analysis," *Veh. Syst. Dyn.*, vol. 54, no. 7, pp. 902-917, 2016.

[29] G. Frøseth, P. Nåvik, and A. Rønnquist, "Operational displacement estimations of railway catenary systems by photogrammetry and the integration of acceleration time series," *Int. J. Railw. Technol*, 2019.

[30] S. Derosa, P. Nåvik, A. Collina, and A. Rønnquist, "Railway catenary tension force monitoring via the analysis of wave propagation in cables," *Proc. Inst. Mech. Eng. F. J. Rail Rapid Transit*, 2020, Art. no. 0954409720941724.

[31] F. Duan, Z. Liu, D. Zhai, and A. Rønnquist, "A Siamese network-based non-contact measurement method for railway catenary uplift trained in a free vibration test," *Sensors*, vol. 20, no. 14, 2020, Art. no. 3984.

[32] Y. Song, Z. Liu, F. Duan, Z. Xu, and X. Lu, "Wave propagation analysis in high-speed railway catenary system subjected to a moving pantograph," *Appl. Math. Model*, vol. 59, pp. 20–38, 2018.

[33] O. Lopez-Garcia, A. Carnicero, and J. L. Marono, "Influence of stiffness and contact modelling on catenary–pantograph system dynamics," *J. Sound Vib.*, vol. 299, no. 4–5, pp. 806–821, 2007.

[34] J. W. Kim, H. C. Chae, B. S. Park, S. Y. Lee, C. S. Han, and J. H. Jang, "State sensitivity analysis of the pantograph system for a high-speed rail vehicle considering span length and static uplift force," *J. Sound Vib.*, vol. 303, no. 3–5, pp. 405–427, 2007.

[35] M. Aboshi, "Influence of wave motion of contact wire on contact force fluctuation (2nd report, experiments in practical catenary–pantograph system," *Trans. Jpn. Soc. Mech. Eng. C*, vol. 84, no. 622, pp. 1896–1903, 1998.

[36] F. Vesali, M. A. Rezvani, and H. Molatefi, "Simulation of the dynamic interaction of rail vehicle pantograph and catenary through a modal approach," *Arch. Appl. Mech.*, vol. 90, pp. 1–22, 2020.

[37] O. V. Van, J. P. Massat, and E. Balmes, "Waves, modes and properties with a major impact on dynamic pantograph–catenary interaction," *J. Sound Vib.*, vol. 402, pp. 51–69, 2017.

[38] M. A. Slawinski, *Seismic Waves and Rays in Elastic Media*. Oxford, UK: Elsevier Science, 2003.

[39] Railway applications-current collection systems-validation of simulation of the dynamic interaction between pantograph and overhead contact line. EN50318, European Committee for Electrotechnical Standardization, CENELEC Central Secretariat, Brussels, 2018

[40] Railway applications. Fixed installations. Electric traction overhead contact lines. BS EN 50119:2009, BSI, London, UK, 2009.

Fuchuan Duan (S'19) received his B.S. degree in electrical information science and technology from Southwest Jiaotong University in 2013, where he is currently pursuing his Ph.D. with the School of Electrical Engineering.

His research interests include finite element modeling, structural dynamics, image processing, and their applications in the design and maintenance of railway pantograph–catenary system.

Zhigang Liu (M'06–SM'16) received his Ph.D. in Power System and its Automation from the Southwest Jiaotong University of China in 2003. He is currently a full Professor at the School of Electrical Engineering, Southwest Jiaotong University. His research interests are the electrical relationship of EMUs and traction, detection, and pantograph–catenary performance assessment in high-speed railways.

He was elected as a Fellow of the Institution of Engineering and Technology (IET) in 2017. He is an Associate Editor of *IEEE Transactions on Neural Networks and Learning Systems*, *IEEE Transactions on Vehicular Technology*, *IEEE Transactions on Instrumentation and Measurement*, and *IEEE Access*. He received the *IEEE TIM's Outstanding Associate Editors* award in 2019 and the *Outstanding Reviewer* award of *IEEE Transactions on Instrumentation and Measurement* in 2018.

Yang Song (S'16–M'19) received his Ph.D. in electrical engineering from Southwest Jiaotong University, Sichuan, China, in 2018. He worked as a Research Fellow with the Institute of Railway Research, School of Computing and Engineering, University of Huddersfield, UK, from October 2018 to September 2019.

He is currently a Postdoctoral Fellow at the Department of Structural Engineering, Norwegian University of Technology, Norway. His research interests involve assessing railway pantograph–catenary interaction, wind-induced vibration of long-span structures of railway transportation, and coupling dynamics in railway engineering.

Stefano Derosa is currently a Ph.D. candidate in the Structural Dynamics group at the Department of Structural Engineering, Norwegian University of Science and Technology, NTNU.

His main task focuses, within the broader field of the structural dynamics of railway catenary systems, on understanding and improving prediction models in local wear of contact lines.

Anders Rønnquist received his Ph.D. from the Norwegian University of Science and Technology, Trondheim, Norway, in 2005.

He is currently a full Professor of the Department of Structural Engineering, Norwegian University of Science and Technology. His research interests include structural dynamics, wind engineering, structural monitoring, and system identification for electric railways.

Donghai Zhai received his Ph.D. degree in traffic information engineering and control from Southwest Jiaotong University, China, in 2003.

From 2003 to 2005 he was employed at IBM China Research Laboratory. Since 2006 he has been associated with Southwest Jiaotong University in the department of software engineering. His research interests include autonomous driving, digital image processing, computer vision, and pattern recognition.